Phase-compensated ultra-bright source of entangled photons

J. B. Altepeter, E. R. Jeffrey, and P. G. Kwiat

Department of Physics, University of Illinois at Urbana-Champaign, 1110 West Green Street, Urbana, IL 61801-3080

altepete@uiuc.edu

Abstract: While the most direct method to increase the brightness of a type-I entanglement source is to increase the collected solid angle of the down-conversion, this leads to effective decoherence caused by an angle-dependent phase shift. Using specially designed compensation crystals, we have reversed this effect and created the brightest source of entangled photons to date, over two million measured pairs per second, recorded while measuring the largest reported violation of Bell's inequality (1239 σ).

OCIS codes: (270.0270) Quantum Optics; (190.0190) Nonlinear Optics.

References and links

1. M. A. Nielsen and I. L. Chuang, *Quantum Computation and Quantum Information* (Cambridge University Press, Cambridge, UK, 2000).
2. R. Raussendorf and H. J. Briegel, "A One-Way Quantum Computer," Phys. Rev. Lett. **86**, 5188–5191 (2001).
3. C. H. Bennett, G. Brassard, C. Crépeaux, R. Jozsa, A. Peres, and W. K. Wooters, "Teleporting an unknown quantum state via dual classical and Einstein-Podolsky-Rosen channels," Phys. Rev. Lett. **70**, 1895–1899 (1993).
4. D. Bouwmeester, J.-W. Pan, K. Mattle, M. Eibl, H. Weinfurter, and A. Zeilinger, "Experimental quantum teleportation," Nature **390**, 575–579 (1997).
5. D. Boschi, S. Branca, F. de Martini, L. Hardy, and S. Popescu, "Experimental Realization of Teleporting an Unknown Pure Quantum State via Dual Classical and Einstein-Podolsky-Rosen Channels," Phys. Rev. Lett. **80**, 1121–1125 (1998).
6. J.-W. Pan, M. Daniell, S. Gasparoni, G. Weihs, and A. Zeilinger, "Experimental Demonstration of Four-Photon Entanglement and High-Fidelity Teleportation," Phys. Rev. Lett. **86**, 4435–4438 (2001).
7. P. G. Kwiat, K. Mattle, H. Weinfurter, A. Zeilinger, A. V. Sergienko, and Y. H. Shih, "New high-intensity source of polarization-entangled photon pairs," Phys. Rev. Lett. **75**, 4337–4341 (1995).
8. P. G. Kwiat, E. Waks, A. G. White, I. Appelbaum, and P. H. Eberhard, "Ultrabright source of polarization-entangled photons," Phys. Rev. A **60**, R773–R776 (1999).
9. C. Kurtsiefer, M. Oberparleiter, and H. Weinfurter, "High-efficiency entangled photon pair collection in type-II parametric fluorescence," Phys. Rev. A **64**(023802) (2001).
10. Y.-H. Kim, M. V. Chekhova, S. P. Kulik, M. H. Rubin, and Y. Shih, "Interferometric Bell-state preparation using femtosecond-pulse-pumped spontaneous parametric down-conversion," Phys. Rev. A **63**(062301) (2001).
11. Y. Nambu, K. Usami, Y. Tsuda, K. Matsumoto, and K. Nakamura, "Generation of polarization-entangled photon pairs in a cascade of two type-I crystals pumped by femtosecond pulses," Phys. Rev. A **66**(033816) (2002).
12. G. Bitton, W. P. Grice, J. Moreau, and L. Zhang, "Cascaded ultrabright source of polarization-entangled photons," Phys. Rev. A **65**(063805) (2002).
13. M. Fiorentino, G. Messin, C. E. Kuklewicz, F. N. C. Wong, and J. H. Shapiro, "Generation of ultrabright tunable polarization entanglement without spatial, spectral, or temporal constraints," Phys. Rev. A **69**(041801) (2003).
14. B.-S. Shi and A. Tomita, "Generation of a pulsed polarization entangled photon pair using a Sagnac interferometer," Phys. Rev. A **69**(013803) (2004).
15. M. Fiorentino, C. E. Kuklewicz, and F. N. C. Wong, "Source of polarization entanglement in a single periodically poled KTiOPO4," Opt. Express **13**, 127 (2005). URL http://www.opticsexpress.org/abstract.cfm?URI=OPEX-13-1-127.
16. P. G. Kwiat, P. H. Eberhard, A. M. Steinberg, and R. Y. Chiao, "Proposal for a loophole-free Bell inequality experiment," Phys. Rev. A **49**, 3209–3220 (1994).

#8740 - $15.00 USD Received 12 September 2005; revised 17 October 2005; accepted 21 October 2005

17. F. N. C. Wong, private communication (2005).
18. A. Joobeur, B. E. A. Saleh, T. S. Larchuk, and M. C. Teich, "Coherence properties of entangled light beams generated by parametric down-conversion: Theory and experiment," Phys. Rev. A **53**, 4360–4371 (1996).
19. N. Boeuf, D. Branning, I. Chaperot, E. Dauler, S. Guerin, G. Jaeger, A. Muller, and A. L. Migdall, "Calculating characteristics of noncollinear phase matching in uniaxial and biaxial crystals," Opt. Eng. **39**, 1016–1024 (2000).
20. S. Castelletto, I. P. Degiovanni, A. Migdall, and M. Ware, "On the measurement of two-photon single-mode coupling efficiency in parametric down-conversion photon sources," New Journal of Physics **6**, 87 (2004).
21. V. G. Dmitriev, G. G. Gurzadyan, and D. N. Nikogosyan, *Handbook of Nonlinear Optical Crystals* (Springer, Berlin, 1999).
22. A. Migdall, "Polarization directions of noncollinear phase-matched optical parametric downconversion output," J. Opt. Soc. Am. B **14**, 1093–1098 (1997).
23. We have not studied the effects of phase compensation in conjunction with single-mode collection optics. However, it is the untested conjecture of the authors that rather than causing decoherence, angle-dependent phases may cause the coupling *efficiency* of the $|HH\rangle$ and $|VV\rangle$ terms to vary independently. The compensators presented here would cause them to vary jointly, with specially designed compensators allowing optimal and balanced coupling.
24. A. G. White, D. F. V. James, P. H. Eberhard, and P. G. Kwiat, "Nonmaximally Entangled States: Production, Characterization, and Utilization," Phys. Rev. Lett. **83**, 3103 (1999).
25. J. B. Altepeter, D. F. V. James, and P. G. Kwiat, *Quantum State Estimation*, vol. 649 of *Lecture Notes in Physics* (Springer, Berlin, 2004).
26. This technique, proposed and first implemented by A. G. White (Univ. of Queensland, Australia), attempts to eliminate some of the loss due to high reflectivity (40%) spectral filters. By placing a QWP between the measurement PBS and the filter-detector assemblies, any reflected light will travel through the quarter waveplate, be reflected at the PBS, be retroreflected by a mirror, and travel back through the PBS toward the filter-detector assembly for a second chance at detection. The effective transmission of the filter is thus increased from 0.6 to $\sim (0.6 + 0.4 \times 0.6) = 0.84$.
27. J. F. Clauser, M. A. Horne, A. Shimony, and R. A. Holt, "Proposed Experiment to Test Local Hidden-Variable Theories," Phys. Rev. Lett. **23**, 880 (1969).

1. Introduction

Entanglement, the quintessential characteristic of quantum mechanics, has been identified as a fundamental resource for quantum information [1] and quantum computation [2]. Though there are several physical systems which have demonstrated entanglement, e.g., photons, atoms, and ions, there exist protocols (such as teleportation [3]) which are only useful for communication when using entangled *photon* states [4, 5, 6]. There have been a number of demonstrations of polarization-entangled photon sources based on down-conversion [7, 8, 9, 10, 11, 12, 13, 14, 15], but most have been limited by small collection apertures. While larger collection apertures lead to brighter sources, they also lead to a degradation in the quality of entanglement. This degradation results from either a fundamentally small entangled solid angle (for Type-II sources [7]) or decoherence which increases with larger collection irises (for Type-I sources [8]). The first proposed solution to this problem [16] interferometrically combines the output of two type-II sources (each operating collinearly) on a polarizing beam splitter. (This can be compared with other interferometric entanglement sources [10, 13].) In this way the spatial and spectral modes of the two possible down-conversion processes are made indistinguishable, though the method has the drawback of requiring interferometric stability; this can be somewhat mitigated by using a stable Sagnac interferometer [14, 17].

Here, we present experimental results for a robust, high-quality, extremely bright, large-aperture double-crystal Type-I source, achieved by installing specially designed crystals which counteract an angle-dependent phase-based decohering effect. This technique has allowed us to simultaneously achieve state fidelities of 97.7% and measured intensities in excess of one million photon pairs per second. By additionally increasing the pump power to the saturation point of our detectors, we obtained a 1239-σ violation of Bell's inequality in under 30 seconds, with an intensity of 2.01×10^6 detected photon pairs per second.

#8740 - $15.00 USD Received 12 September 2005; revised 17 October 2005; accepted 21 October 2005

2. Two-crystal source of polarization-entangled photons

Our experiment utilizes Type-I down-conversion within two adjacent, orthogonally oriented BBO crystals [8]. Within the first crystal, a horizontally polarized 351-nm pump photon ($|H\rangle$) down-converts into two 702-nm vertically polarized daughter photons ($|VV\rangle$). The second crystal is identically cut, but rotated by 90° about the pump axis, so that $|V\rangle$ down-converts into $|HH\rangle$. Because these crystals are thin compared to the coherence length of the pump, the down-converted states produced from the same pump photon interfere, allowing the 351-nm pump state $\cos(\varepsilon)|V\rangle + e^{i\phi}\sin(\varepsilon)|H\rangle$ to down-convert into the two-photon 702-nm state $\cos(\varepsilon)|HH\rangle + e^{i\phi}\sin(\varepsilon)|VV\rangle$, which is emitted into a cone with a $\sim 3°$ opening angle outside the crystals. The phase factor ϕ is determined by the exact path that the down-converted photons take within the down-conversion crystals (calculating ϕ will be addressed in the next section). Figure 1(a) details the experimental apparatus used to create and measure entangled states.

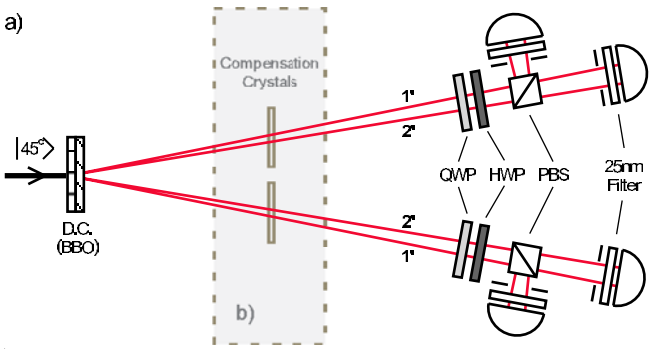

Fig. 1. Entangled photon source. (a) A 45°-polarized 351-nm pump beam down-converts in two adjacent nonlinear crystals (BBO) into the two-photon state $|\psi(\phi)\rangle = \frac{1}{\sqrt{2}}\left(|HH\rangle + e^{i\phi}|VV\rangle\right)$. The phase factor ϕ depends on the angle of the down-conversion photons within the crystals, such that the states corresponding to paths 1' and 2' are $|\psi(1')\rangle$ and $|\psi(2')\rangle$, respectively. The addition of these states results in effective decoherence. The use of larger collection apertures increases the effect. (b) By placing additional specially designed birefringent crystals into the down-conversion path, this phase variation can be compensated for, largely eliminating the decohering effect of large collection apertures. The quarter waveplate (QWP), half waveplate (HWP), polarizing beam splitter (PBS) combinations in each arm allow projection into any separable polarization basis. A sequence of these projections allows complete tomographic reconstruction of any two-qubit density matrix. Quoted high count rates were collected using 9-mm irises (120 cm from the source) and 25-nm (FWHM) frequency filters.

3. Angle-dependent birefringent phases

3.1. Calculating the angle-dependent phase from an arbitrary birefringent crystal

Though many groups have performed calculations of down-conversion in a single nonlinear crystal [18, 19, 20], here we present a specific and complete calculation of the angle-dependent phase differences necessary to design a compensated two-crystal entanglement source. In general, calculating the phase that a monochromatic photon accumulates from a birefringent crystal at arbitrary orientation requires three separate but interconnected calculations: the extraordinary phase Φ_e, the ordinary phase Φ_o, and the extra phase Φ_Δ that the extraordinary beam accumulates *outside* the crystal.

#8740 - $15.00 USD Received 12 September 2005; revised 17 October 2005; accepted 21 October 2005

To simplify this calculation, we assume the $\hat{z}$-axis to be normal to the crystal surface, the incident photon to be travelling in the $\hat{x}$-$\hat{z}$ plane with positive $\hat{z}$- and non-negative $\hat{x}$-momenta, and the faces of the crystal to be parallel and transversly unbounded. We define the following angles, vectors, and variables (see Fig. 2, and note that a ˆ symbol indicates a unit vector):

$\hat{k}_\alpha$	Incident photon's unit momentum vector outside of the crystal.
$\hat{\kappa}_o$	Unit momentum vector for ordinarily polarized light inside the crystal.
$\hat{\kappa}_e$	Unit momentum vector for extraordinarily polarized light inside the crystal.
α	Angle between $\hat{z}$ and $\hat{k}_\alpha$.
ψ_o	Angle between $\hat{z}$ and $\hat{\kappa}_o$.
ψ_e	Angle between $\hat{z}$ and $\hat{\kappa}_e$.
$\hat{O}$	Crystal optic axis.
$\hat{S}_o$	Ordinary Poynting vector inside the crystal. Always equal to $\hat{\kappa}_o$.
$\hat{S}_e$	Extraordinary Poynting vector inside the crystal.
β	Angle between $\hat{z}$ and $\hat{S}_e$.
ρ	Angle between $\hat{S}_e$ and $\hat{\kappa}_e$.
Δ	Free-space distance that the extraordinary but not the ordinary beam must travel.
n_o, n_e	The crystal's ordinary and extraordinary indices of refraction.
$n^e(\theta)$	The index of refraction for a direction which is angle θ from the optic axis.

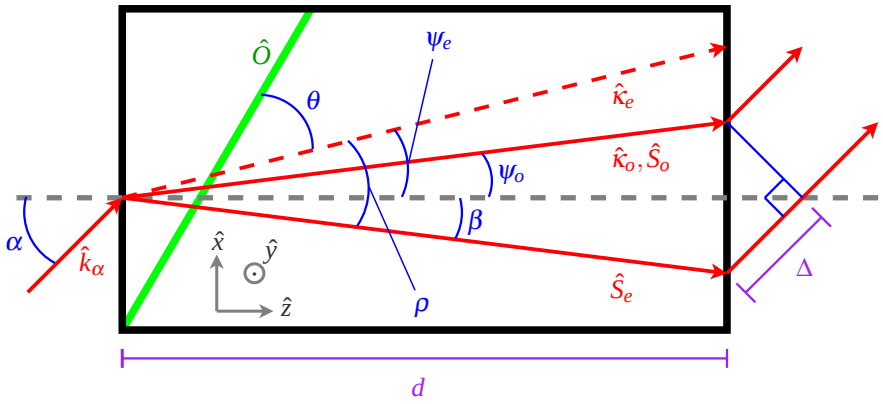

Fig. 2. Diagram illustrating all relevant vectors, angles, and variables used for calculating angle-dependent phase differences due to birefringent crystals. Arbitrarily polarized light is incident from the left onto a negative uniaxial crystal (e.g., BBO) with its optic axis ($\hat{O}$) in the plane of the page.

Using these definitions, we can build the formulae necessary to compute the relevant phases. First, we write down the formulae based on Snell's Law and basic birefringence [21]:

$$\psi_o \equiv \operatorname{asin}\left(\frac{\sin(\alpha)}{n_o}\right), \tag{1}$$

$$\psi_e \equiv \operatorname{asin}\left(\frac{\sin(\alpha)}{n^e(\theta)}\right), \tag{2}$$

$$n^e(\theta) \equiv n_o \sqrt{\frac{1+\tan^2\theta}{1+\left(\frac{n_o}{n_e}\tan\theta\right)^2}}. \tag{3}$$

#8740 - $15.00 USD Received 12 September 2005; revised 17 October 2005; accepted 21 October 2005

In birefringent materials, the extraordinary beam's Poynting vector ($\hat{S}_e$) deviates from its momentum vector ($\hat{\kappa}_e$) by an angle ρ:

$$\rho = \left(\theta - \operatorname{atan}\left[\frac{n_o^2}{n_e^2}\tan\theta\right]\right)\operatorname{sgn}(n_o - n_e). \tag{4}$$

$\hat{S}_e$ dictates the physical path of the light as it travels through the crystal, and more importantly, when and where it *exits* the crystal. This vector is further from the optic axis than $\hat{\kappa}_e$ for negative uniaxial crystals ($n_o > n_e$), and closer for positive uniaxial crystals ($n_o < n_e$). Figure 2 shows the special case where $\hat{S}_e$ is in the plane of incidence.

We are now ready to compute in radians the three phases relevant to the problem, by multiplying the optical path length in waves by a factor of $\frac{2\pi}{\lambda}$ (λ is the wavelength of the photon *outside* of the crystal):

$$\Phi_o = \frac{d}{\cos(\psi_o)} n_o \left(\hat{S}_o \cdot \hat{\kappa}_o\right) \frac{2\pi}{\lambda} = \frac{d}{\cos(\psi_o)} n_o \frac{2\pi}{\lambda}, \tag{5}$$

$$\Phi_e = \frac{d}{\cos(\beta)} n^e(\theta) \left(\hat{S}_e \cdot \hat{\kappa}_e\right) \frac{2\pi}{\lambda}, \tag{6}$$

$$\Phi_\Delta = \frac{2\pi}{\lambda}\Delta = \frac{2\pi}{\lambda}\left(\frac{d}{\cos(\psi_o)}\hat{S}_o \cdot \hat{k}_\alpha - \frac{d}{\cos(\beta)}\hat{S}_e \cdot \hat{k}_\alpha\right). \tag{7}$$

The dot product in Eq. 5 and Eq. 6 accounts for the fact that although the light travels along $\hat{S}$, its wavefronts are perpendicular to and determined by $\hat{\kappa}$, creating a smaller effective optical path length by a factor of the cosine of the angle between these vectors. In Eq. 5, this factor is 1, but for the extraordinary case—Eq. 6—this can be a large effect. The distance Δ depends entirely on where $\hat{S}_o$ and $\hat{S}_e$ enter and exit the crystal, which can be quite complicated for the general case where these vectors are not in the plane of incidence: We project these two vectors (using a dot product) onto $\hat{k}_\alpha$. The difference between these projections is the distance Δ.

3.2. Calculating the angle-dependent phase from compensated down-conversion

Now that we are able to compute the ordinary and extraordinary phases within the crystal, we can calculate the phase ϕ as a function of the signal direction outside of the crystals, $\hat{k}_\alpha$. We first make the approximations that the signal and idler photons are "born" in the center of their respective crystals, travel in directions which are completely symmetric about the pump beam, are ordinarily polarized in their own crystal, and are extraordinarily polarized in the remaining crystal (this approximation is close to correct, but see [22] for a complete calculation). Both the $|VV\rangle$ and $|HH\rangle$ terms receive an equal ordinary phase in their own crystals, which we can neglect as a global phase. The $|VV\rangle$ photons born in the first crystal together receive a net additional extraordinary phase in the second crystal equal to

$$\phi_{\mathrm{dc}}\left(\hat{k}_\alpha\right) = 2\left(\Phi_{\mathrm{dc},e} + \Phi_{\mathrm{dc},\Delta}\right), \tag{8}$$

double the phase accumulated by just one of the daughter photons. (Note that the terms in Eq. 8 implicitly depend on $\hat{k}_\alpha$). This makes the final entangled state for a 45°-polarized pump beam:

$$|\psi_{\hat{k}_\alpha}\rangle = \frac{1}{\sqrt{2}}\left(|HH\rangle + e^{i2\left(\Phi_{\mathrm{dc},e}+\Phi_{\mathrm{dc},\Delta}\right)}|VV\rangle\right). \tag{9}$$

Because experimental setups use finite size irises which accept a range of $\hat{k}_\alpha$, the state passed by the irises can be described by the unnormalized state:

$$|\psi\rangle_{\mathrm{Iris}} = \int_{\mathrm{Iris}} |\psi_{\hat{k}_\alpha}\rangle |\hat{k}_\alpha\rangle d\hat{k}_\alpha. \tag{10}$$

#8740 - $15.00 USD Received 12 September 2005; revised 17 October 2005; accepted 21 October 2005

Because all pairs that pass through the irises are measured together, the actual state measurement traces over direction, producing the density matrix:

$$\rho = \int_{\text{Iris}} |\psi_{\hat{k}_\alpha}\rangle\langle\psi_{\hat{k}_\alpha}| d\hat{k}_\alpha. \tag{11}$$

Averaging over the different emission directions averages over the relative phase, leading to an effective decoherence. (Note that these calculations apply only to irises which collect multiple modes; see [23].) The angle-dependent phase can be corrected with appropriate birefringent compensation crystals. These are different than the special case of down-conversion crystals; here all photons always travel through the *entire* crystal (e.g., no photons are born in the middle of a crystal). If we use compensation crystals parallel to the down-conversion crystals, the phase due to two compensation crystals, one in each arm, with optic axes in the horizontal plane, is

$$\phi_c\left(\hat{k}_\alpha\right) = 2\left(\Phi_{c,o} - \Phi_{c,e} - \Phi_{c,\Delta}\right), \tag{12}$$

with the final compensated state equal to

$$|\psi_{\text{comp},\hat{k}_\alpha}\rangle = \frac{1}{\sqrt{2}}\left(|HH\rangle + e^{i(\phi_{\text{dc}}+\phi_c)}|VV\rangle\right). \tag{13}$$

3.3. Designing compensation crystals

When the principles of the previous two subsections are applied to our experimental system, we are able to plot the theoretical angle-dependent phase difference due to the down-conversion crystals (see Fig. 3(a)). In order to design crystals to compensate the predicted slope, we need to optimize these compensation crystals such that the sum of the phasemaps from the down-conversion and the compensation crystals is as flat as possible.

As a starting point, we decided to use BBO cut at the same angle as the down-conversion crystals. This is a choice of experimental convenience, as there is a continuum of virtually equivalent choices accessible by making a tradeoff between optic-axis angle and crystal thickness. If the optic axis is fixed at 33.9° (from crystal normal) and the thickness is optimized, we find that a thickness of 245-μm is ideal (phasemap also shown in Fig. 3(a)). Figure 3(b) shows the expected sum of the first two phasemaps, an extremely flat function as compared to the original down-conversion phasemap; Fig. 3(c) shows the theoretical prediction of the simultaneously bright and high-fidelity compensated state (only the absolute value of the state is shown, as it is the coherence which is important rather than the particular value of the phase between $|HH\rangle$ and $|VV\rangle$).

4. Measurements of phase-based decoherence and compensation

4.1. Measurement of the angle-dependent phasemap

Figures 3(d-e) show the experimental measurement of the phasemap over a 1-cm square area 120 cm from the down-conversion crystals. Each point on the figure was calculated by taking a complete state tomography [24, 25] (a series of separable polarization measurements which allow one to infer the quantum state of an ensemble of identical particles) using small irises ($\sim$ 2 mm) centered at the appropriate position. There is a significant (17%) difference in slope between the theoretical and experimental phasemaps (Figs. 3(a,e)), indicating that one or more of our theoretical assumptions may have been unjustified. Even so, this first attempt at a compensation model has improved our phase flatness by a factor of seven, leading to dramatic increases in state quality and brightness.

#8740 - $15.00 USD Received 12 September 2005; revised 17 October 2005; accepted 21 October 2005

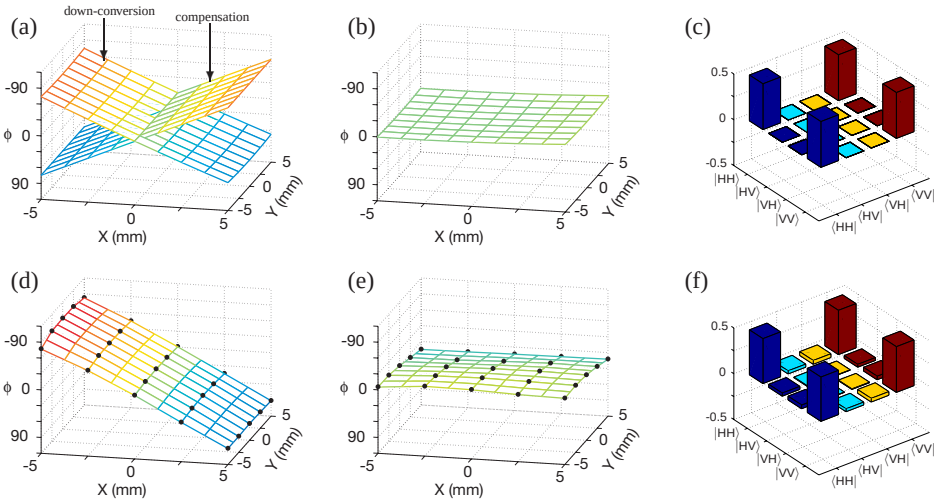

Fig. 3. Theoretical (a-b) and experimental (d-e) plots of the phase difference ϕ as a function of signal direction $\hat{k}_\alpha$, combined with the predicted (c) and measured (f) density matrices. To match experimentally collected data, the direction $\hat{k}_\alpha$ is represented as a transverse position in space ~ 120 cm from the down-conversion crystals. Here, $x = 0$, $y = 0$ corresponds to the central 702-nm down-conversion directions, $\sim 3^\circ$ (6.35 cm) from the pump axis. (a) The phasemap due solely to the down-conversion crystals (each 600-μm thick, 33.9° optic axis, BBO), superimposed with the phasemap due to two BBO compensation crystals, one in each arm, each 245 μm thick and cut with a 33.9° optic axis. The slope of each phasemap is approximately $\pm 14^\circ$ per mm. (b) The sum of both phasemaps from (a). The flat character indicates that approximately the same entangled state will be present at each position on this plot, corresponding to a high-fidelity state measured using large irises. (c) The theoretically predicted density matrix that would result from a measurement over this flat phase surface, using 1-cm diameter irises. (d) Experimentally measured phase for the uncompensated configuration. Each black dot represents an experimental measurement of this phase, extracted from the result of a full state tomography. The mesh graphically represents these points by linearly connecting nearest neighbors. The phase difference is nearly linear, approximately 17° per millimeter, and varying in the radial direction out from the pump beam axis. (e) The compensated configuration. The surface is very flat, with a maximum slope of less than 3°/mm, and a total phase variation of approximately 25° over a centimeter, a seven-fold improvement over the uncompensated case. (f) The experimentally recorded density matrix (absolute value shown here) describing the ultra-bright entangled state: 1.02×10^6 measured pairs per second, 97.7% fidelity with a maximally entangled state.

4.2. Iris size and decoherence

The bottom-line test of this compensation scheme is to compare the fidelity between a target pure state and the experimentally measured state, as a function of changing iris sizes, using both compensated and uncompensated states. Fidelity between a pure state ($|\psi\rangle$) and a mixed state (ρ) is defined as

$$F(|\psi\rangle, \rho) \equiv \langle\psi|\rho|\psi\rangle. \tag{14}$$

Fig. 4 shows the state fidelity as a function of iris size for both the standard and compensated cases. Because state intensity is proportional to solid angle, a linear increase in iris diameter roughly corresponds to a quadratic increase in photon pairs.

#8740 - $15.00 USD Received 12 September 2005; revised 17 October 2005; accepted 21 October 2005

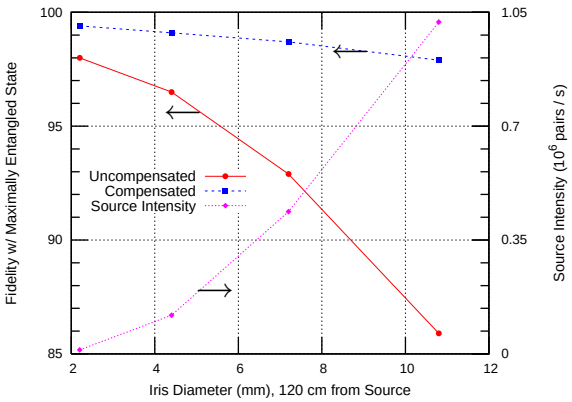

Fig. 4. The effects of iris size on the fidelity and rate of measured entangled states. Note that for this measurement, the diameters of *both* irises are adjusted, with each positioned in the plane normal to the pump direction and 120 cm from the down-conversion crystals. Shown here are both the standard (uncompensated) and compensated configurations. The *y*-axis on the right describes the detected source intensity (for a 280-mW pump and 25-nm filters), quadratically increasing as a function of iris size.

5. The ultra-bright source

5.1. Efficiency optimization, crystal damage, and high counts

In order to measure this ultra-bright source, it was necessary to address the problem of detector saturation. Because our detectors have a maximum useful rate of approximately 4×10^6 singles counts per second, measuring high coincidence count rates requires high detection efficiencies. Taking advantage of both the high collection efficiency of large irises and a novel reflection technique [26], we achieved detection efficiencies in excess of 30%. (This efficiency is due to detector quantum efficiency ($\sim 65\%$ for the SPCM AQR-14), iris collection efficiency ($\sim 70\%$ for 9-mm irises), reflection losses from the interference filters ($\sim 84\%$ [26]), saturation losses due to the 30-ns dead-time of the detectors (up to $\sim 5\%$, depending on the count rate), and other reflection and absorption losses due to miscellaneous optics.) In addition, using a polarizing beam-splitter and two detectors in each arm (see Fig. 1), we were able to simultaneously measure a complete basis of four separable projectors at a time, giving each singles count a chance to contribute to a coincidence.

5.2. Results

Using $\sim$ 9-mm irises, a pump power of 280 mW, and the compensation scheme described above, quantum state tomography reconstructed a state having a $97.7\% \pm 0.1\%$ fidelity with a maximally entangled state and an average intensity of 1.02×10^6 pairs per second. While this indicates a bright, high-quality entangled state, we took a series of measurements of Bell's inequalities [27] in order to demonstrate not only the state's quality but also the extremely short time in which precise measurements can be collected. We measured a violation of 2.7260 ± 0.00336 (216 σ) in 0.8 s of total measurement time, and a violation of 2.7252 ± 0.000585 (1239 σ) in 28 s with an average measured intensity of 2.01×10^6 pairs per second. (We should note that because the statistical errors on these values are extremely low, it is very likely that uncharacterized systematic errors are dominating these measurements.)

For this last result, we applied 310 mW of pump power to the down-conversion crystals. This level of power resulted in both damage to the down-conversion crystals (or at least their

#8740 - $15.00 USD Received 12 September 2005; revised 17 October 2005; accepted 21 October 2005

antireflection coatings) and high saturation of the detectors. Because of these saturation effects and our detection inefficiency, the entangled pairs actually produced substantially exceed the number measured (correcting for a 30% detection efficiency near saturation, we estimate that the actual rate of entangled-state *production* into 9-mm irises and 25-nm filters exceeds 20×10^6 entangled pairs per second).

6. Conclusion

Existing type-I sources of entanglement stand to be dramatically improved by incorporating custom compensation crystals, the principles of which have already been modeled, tested, and reported in this paper. Those models, however, rely on a number of approximations (e.g., monochromatic light, symmetric down-conversion, perfectly extraordinary polarization in the second crystal), and improvements in this technique (even given the seven-fold increase in phase flatness, there is a sizable phase slope remaining) will require a more careful theoretical treatment of the problem. Ultimately, continuing to push the limits of source brightness will require new detector solutions, as the source described in this manuscript is currently limited only by how quickly our detectors can count.

Acknowledgments

This work was supported by the National Science Foundation (Grant No. EIA-0121568) and the MURI Center for Photonic Quantum Information Systems (ARO/ARDA program DAAD19-03-1-0199).

#8740 - $15.00 USD Received 12 September 2005; revised 17 October 2005; accepted 21 October 2005